Stress recovery and cyclic behaviour of an Fe-Mn-Si shape memory alloy after multiple thermal activations

E. Hosseini[1,2], E. Ghafoori[1,3,*], C. Leinenbach[1], M. Motavalli[1,4], S.R. Holdsworth[1,2]

[1] Empa, Swiss Federal Laboratories for Material Science and Technology, Überlandstrasse 129, CH-8600 Dübendorf, Switzerland

[2] Inspire Centre for Mechanical Integrity, c/o Empa, CH-8600 Dübendorf, Switzerland

[3] Swinburne University of Technology, VIC 3122 Hawthorn, Melbourne, Australia

[4] University of Tehran, 16th Azar Street, Tehran, Iran

Abstract

The stress recovery and cyclic deformation behaviour of Fe–17Mn–5Si–10Cr–4Ni–1(V,C) shape memory alloy (Fe-SMA) strips, which are often used for pre-stressed strengthening of structural members, were studied. The evolution of recovery stress under different constraint conditions was studied. The results showed that the magnitude of the tensile stress in the Fe-SMA member during strengthening can have a signification effect on the final recovery stress. The higher the tensile stress in the Fe-SMA (e.g., caused by deadload or thermal expansion of parent structure during heating phase), the lower the final recovery stress. Furthermore, this study investigated the cyclic behaviour of the pre-stressed alloy followed by a second thermal activation. Although the magnitude of the recovery stress decreased during the cyclic loading, the second thermal activation could retrieve a significant part of the relaxed recovery stress. This observation suggests that the relaxation of recovery stress is due to a reversible phase transformation-induced deformation (i.e., forward austenite-to-martensite transformation) rather than an irreversible dislocation-induced plasticity. Retrieval of the relaxed recovery stress by the reactivation process has important practical implications as the pre-stressing loss in pre-stressed civil structures can be simply recovered by reheating of the Fe-SMA elements.

---

[*]Corresponding author. Tel.: +41 58 765 4935.
E-mail address: elyas.ghafoori@empa.ch (Elyas Ghafoori).

1.   Introduction

Shape memory alloys (SMAs) are smart metals that can retrieve their shape after being de-
formed through an activation process which includes heating and cooling. Ni-Ti SMAs,
which are the most commonly used SMAs, have different applications such as medical and
aerospace devices. Fe-Mn-Si based SMAs have gained much attention because of their rela-
tively low production cost and good mechanical properties [1]. Because of these favourable
characteristics, Fe-Mn-Si SMAs are considered in mechanical [2] and civil engineering appli-
cations [3]. The shape memory effect (SME) in Fe-Mn-Si alloys is a result of a stress-induced
forward phase transformation from austenite-to-martensite at low temperature and its reverse
upon heating at higher temperatures [4]. An SMA element can be used as a pre-stressing el-
ement in civil/mechanical engineering applications when it is constrained during the activa-
tion process. There have been many studies on utilization of SMAs for pre-stressed confine-
ment of concrete girders [5], concrete columns [6] and steel tensile members [7].

A novel Fe-17Mn-5Si-10Cr-4Ni-1(V,C) SMA, which will be hereafter referred to as Fe-
SMA, has been recently developed at Empa [8-11]. Previous works on the corrosion [12], re-
covery stress [9], creep/relaxation [13] and phase transformation [3] of the alloy showed its
suitability for civil and mechanical engineering applications. Pre-stressed elements made of
fibre-reinforced polymer (FRP) have been already proven to be very effective in increasing
the performance of concrete [14, 15] and metallic [16-19] structures. However, the easy pre-
stressing method of the Fe-SMA elements offers clear advantages over the complex pre-
stressing techniques required for FRP composites [20, 21]. Figure 1 schematically presents
the general concept of pre-stressed strengthening of a structural member (which is also called
"parent structure") using the Fe-SMA strips. The different steps of pre-straining (Figure 1.a),
anchoring (Figure 1.b) and thermal activation (Figure 1.c) are illustrated. Finally, Figure 1.d
shows the expected stress state in the form of compression in the parent structure and tension
in the Fe-SMA strip after the activation. It has been shown in previous studies that applica-

tion of a compression stress to structural members (using pre-stressed elements) can enhance the flexural capacity [22], buckling strength [16] and fatigue behaviour [23, 24] of civil structures.

While there are studies on the phase transformation and the recovery stress of Fe-SMA (e.g., [25-27]), the mechanical behaviour of activated Fe-SMA subjected to cyclic loading has not yet been studied. This is while it is important for design assessments to acknowledge the mechanical response of the Fe-SMA after activation.

The present study first reports observations from conducted experiments for characterisation of the as-received Fe-SMA strips in terms of tensile strengths, thermal expansion behaviour and stress recovery response. Later it examines the behaviour of the activated Fe-SMA strips under cyclic loading. Moreover, this work studies the effect of a second activation on the behaviour of the Fe-SMA strips. The test results presented in this work are expected to be helpful for design of pre-stressed retrofit systems for mechanical and civil engineering applications.

2.   Material

The investigated Fe-SMA in this study was received in the form of 1.5mm thick sheets with a width of 100mm. The production process for the sheets included induction melting and casting of large ingots under atmospheric conditions, stepwise hot pressing to a thickness of 15mm, hot rolling to a thickness of 3mm, solution treatment, ageing, and finally cold rolling process. More details about the manufacturing process can be found in [11].

The nominal chemical composition of the alloy is Fe–17Mn–5Si–10Cr–4Ni–1(V,C) (mass%) [28]. Figure 2 shows the microstructure of the as-received Fe-SMA etched with a solution of C_2H_5OH (96%)/HNO_3(65%)/HCl (32%) with the ratio of 17/2/1. The alloy has a polycrystalline microstructure with an average grain size of approximately 11µm. Some of the grains

contain large bands, which are twins, while many grains contain very fine bands, which are presumably ε-martensite.

Note that the changes in the microstructure of the alloy due to mechanical and thermal loading have been already studied using scanning electron microscopy (SEM), electron backscattering diffraction (EBSD) and X-ray diffraction (XRD) techniques [9-11, 13, 27, 28].

3.   Experimental details

A set of dog-bone shaped tensile specimens with a gauge length of 25mm and cross-section of 10×1.5mm^2 was manufactured. The dog-bone specimens were extracted longitudinal to the rolling direction of the Fe-SMA strips, using electro discharge machining. A servo-hydraulic uniaxial testing machine equipped with an induction heating system was employed for conducting of the experiments (see Figure 3). A spring-loaded side-entry extensometer with a datum leg spacing of 15mm was attached to the central part of the specimen gauge length for strain measurement. Force was monitored by the built-in load cell of the testing machine. Feedback from a type-K thermocouple (spot-welded to the centre of specimen gauge length) was used for control of the induction heating and an air cooling system for careful control of the specimen temperature. A summary of the conducted experiments is given in Table 1 and further described in the followings.

3.1 Material characterisation

Tensile behaviour: The room temperature tensile properties of the as-received Fe-SMA were measured at a strain rate of 0.15%s^{-1}. For strains smaller than 10%, the test was controlled based on direct feedback from the side-entry extensometer. For larger strains, because of the measurement limitation of the extensometer, the test continued under a machine crosshead displacement rate of 0.075mms^{-1} which is approximately equivalent to the strain rate of 0.15%s^{-1} in the gauge length.

Thermal expansion behaviour: The thermal expansion behaviour of the as-received Fe-SMA was investigated for the temperature range of 25-160°C. The evaluation included monitoring the thermal strain development in the specimen under a zero-stress loading condition while heating up from room temperature to 160°C and then cooling down to room temperature again. In order to remove the possible strain contribution from shape recovery of the SMA after cold rolling, the specimen was heated up to 170°C prior to the thermal strain measurement.

Stress recovery behaviour: The Fe-SMA specimens were first loaded to 2% tensile strain at room temperature. Subsequent unloading of the specimens indicated accumulation of ~1.3% tensile pre-strain in the Fe-SMA. For thermal activation, the specimens were kept under either constant total strain or constant mechanical strain ($\varepsilon_{mechanical} = \varepsilon_{total} - \varepsilon_{thermal}$) during heating and cooling processes with a constant temperature transient rate of 2°C/min or 30°C/min. For the mechanical strain-controlled activation, a tensile strain equivalent to its thermal expansion was applied to the SMA during the heating, while the equivalent compressive strain was imposed to the SMA during the cooling process. The mechanical strain includes all the strain components (e.g. due to SME, creep and elastic-loading) except the thermal strain contribution. In order to prevent buckling of the specimens (during the early part of heating), a tensile stress of 50MPa was applied to the specimen before the start of the activation process [9]. The activation process (i.e., heating and cooling processes) retrieved a portion of the pre-accumulated strain and recovered a significant tensile stress in the specimens.

3.2 Cyclic deformation response of the Fe-SMA after activation

Fe-SMA reinforced civil engineering structures are typically subjected to external cyclic loading, and therefore, cyclic stresses are expected to superimpose on to the recovered stress in the Fe-SMA during the service life of such structures. As the thin Fe-SMA strip has insignificant effect on the global stiffness of large civil structures, the imposed cyclic loading on the Fe-SMA is assumed to have a strain-control characteristic. Laboratory simulation of such a con-

dition has been realised in a set of tests in this study. In these tests, after the activation process, a strain-control cyclic loading was applied to the Fe-SMA to evaluate the mechanical response of the activated Fe-SMA subjected to cyclic loading.

The test campaign focused on two strain ranges of 0.035% and 0.070% with frequency of 10Hz for two million cycles. The strain ranges of 0.035% and 0.070% are aimed to represent the common (service) strain ranges that are subjected to pre-stressing elements in steel [7, 29] and concrete [9] structures, respectively. The testing matrix was further complemented with two additional tests, one with a strain range of 0.105% and frequency of 10Hz and the other with strain range of 0.070% and frequency of 2mHz (2×10^{-3}Hz). The observations from the cyclic loading were exploited to understand the mechanical response of the activated Fe-SMA.

3.3 Second activation and subsequent cyclic loading

Two of the cyclic tests described in Section 3.2 were chosen to be followed by a second thermal activation. At the end of cyclic loading, the specimens were kept under a constant total strain condition while were heated up to 160°C and subsequently cooled down to room temperature. The tests were then continued by additional strain-controlled cyclic loading to evaluate the cyclic response of the Fe-SMA after the second activation.

3.4 Final tensile testing

Finally and after the end of cyclic loading, the specimens were loaded up to failure to determine the effect of the activation process and cyclic deformation on tensile strength and elongation of the Fe-SMA. The tensile loading was conducted under a constant strain rate of 0.15%s^{-1} for strains smaller than 10% and continued up to failure under machine crosshead displacement rate of 0.075mms^{-1} ($\sim \dot{\varepsilon}$=0.15%s^{-1}).

4. Results and discussion

4.1 Tensile testing

Figure 4 presents the observations from uniaxial tensile testing of the as-received Fe-SMA strips. The determined values of elastic modulus, limit of proportionality ($\sigma_{0.01}$), 0.2% proof stress ($\sigma_{0.2}$), tensile strength and elongation are indicated in the figure. The early inelastic response, which can be observed in Figure 4, is assumed to be due to the austenite-to-martensite phase-transformation rather than dislocation induced plasticity [10]. The ultimate tensile strength and elastic modulus of 1015MPa and 173GPa determined in this study are larger and smaller than the 993MPa and 200GPa observed in [10], respectively.

4.2 Thermal expansion behaviour

The thermal expansion behaviour of the Fe-SMA material in an austenitic state has been illustrated in Figure 5 and can be given by:

$$\Delta\varepsilon_{th,25°C} = 1.49\times10^{-5}\left(\theta-25\right) + 3.09\times10^{-8}\left(\theta-25\right)^{2} - 1.09\times10^{-10}\left(\theta-25\right)^{3} \tag{1}$$

where θ is the temperature in degree Celsius. As expected, the thermal expansion of the as received Fe-SMA with an austenite structure [30] is similar to that of other austenitic steels.

4.3 Stress recovery behaviour

The Fe-SMA recovered stress after the thermal activation process depends on the pre-straining and thermal activation conditions. Lee et al. [28] have investigated the influence of different elastic restraints on the formation of the recovery stress in Fe-SMAs. Their observations have shown that the recovery stress is maximum when the Fe-SMA element is fully constrained by a parent structure with infinite stiffness (i.e., rigid restraint) during the activation process. The recovery stress, however, reduces if the parent structure has a finite stiffness (i.e., elastic restraint).

By assuming that a Fe-SMA pre-stressing element is anchored to a very stiff parent structure (e.g., see the structural member shown in Figure 1), the activation process is under a rigid restraint condition (i.e. total strain-control) provided that the temperature of the parent structure does not change during the activation process. However, for the heating condition in which the temperature of both the Fe-SMA element and the parent structure simultaneously changes during the temperature transients, the activation is not any more under a constant total strain condition and is affected by the thermal expansion behaviour of the parent structure. Therefore, for the case where both the Fe-SMA element and the parent structure experience an identical heating and cooling history (e.g. homogeneous temperature distribution), the Fe-SMA undergoes a total tensile and compressive strain during heating and cooling processes, respectively ($\Delta\varepsilon_{tot} = \Delta\varepsilon_{th(parent\ structure)}$). Provided that both the Fe-SMA element and the parent structure have an identical thermal expansion coefficient, the activation takes place under constant mechanical strain ($\Delta\varepsilon_{mech} = \Delta\varepsilon_{tot} - \Delta\varepsilon_{th} = 0 \rightarrow \Delta\varepsilon_{tot} = \Delta\varepsilon_{th}$).

Figures 6.a and 6.b present the observed stress recovery behaviour of the pre-strained Fe-SMA during activation under total and mechanical strain-control for two different temperature transient rates. For the tests with mechanical strain-controlled activation, the total strain during the thermal transient varies based on the relationship given by Equation 1.

The presented results in Figure 6 show that both temperature transient rates result in approximately identical final recovery stress values. Furthermore, a comparison between the recovery stresses achieved by different activation strategies indicates that the final recovery stress is higher when the activation is under total strain-control. For mechanical strain-controlled activation, a larger recovery stress is formed during the heating process compared to that for total strain-controlled activation. During the cooling process, a substantial stress recovery is achieved for activation under total strain-control, while no further stress increase was observed for mechanical strain-controlled activation. It is therefore interesting to see that the finally recovered stress under total strain-control is almost twice that developed under mechan-

ical strain-control. This observation implies that activation of the Fe-SMA element while it is subjected to some extent of tensile stress (e.g., due to thermal expansion of the parent structure or dead-loads) will result in a decreased final recovery stress. In the following, more details about activation under total and mechanical strain-controlled conditions are given.

For total strain-controlled activation, the stress variation during the thermal transient is a result of two simultaneous phenomena of phase transformation and thermal expansion/contraction. At the beginning of heating and below 35°C, the dominance of thermal expansion over the phase transformation effect reduces the stress in the Fe-SMA. During further heating, the phase transformation is more dominant and higher stresses are developed. More significant stress development is observed during the cooling phase where thermal contraction also helps to increase the stress. The decreasing slope of stress increase during cooling at lower temperatures in Figure 6.b is most likely due to time-dependent relaxation and to some extent of austenite-to-martensite phase transformation.

Regarding the activation under mechanical strain-control, based on [28], the main factor determining the final recovery stress is the amount of martensite that transforms back to austenite during the heating process and the induced strain. The applied strain during the heating process of the activation was fully compensated during the cooling phase ($\Delta\varepsilon_{tot} = \Delta\varepsilon_{th}$) and therefore does not directly influence the final recovery stress. Lee et al. [10] have proposed a stress-temperature phase diagram giving estimations for the austenite start, austenite finish and martensite start temperatures (A_s, A_f and M_s lines respectively). A schematic of such a stress-temperature phase diagram is presented in Figure 7 which shows that the A_s temperature increases with increase of the stress level. From Figure 6.b, a stress level of approximately 50MPa and 100MPa were respectively generated under total- and mechanical strain-control during the heating process at θ=60°C (with 2°C/min). Points A and B in Figure 7 represent these two stress-temperature coordinates. It can be seen that while the reverse transformation is expected to have already started under total strain-control (point A), no martensite-to-

austenite phase transformation is expected to occur for the specimen under mechanical strain-control at 60°C (point B).

During heating, and for temperatures higher than 60°C, some extent of reverse phase transformation (martensite-to-austenite) takes place for the specimen activated under mechanical strain-control. It can be shown that for all temperatures, total strain-control results in lower stress levels which are closer to the A_f line. The latter then leads to a larger extent of martensite-to-austenite phase transformation which consequently gives higher final recovery stresses after cooling. Note that the aim of presenting Figure 7 is only to qualitatively show the effect of stress level during the activation process on the magnitude of the reverse phase transformation, and more details regarding the methodology for determination of the A_s, A_f and M_s lines are given in [10].

This observation has important practical implications. It can be concluded that for Fe-SMA pre-stressing elements which are anchored to structural members, employment of a heating methodology that only increases the temperature of the Fe-SMA element and not the parent structure enhances the final obtained recovery stress. Passing a high electrical current through the Fe-SMA element can therefore be considered as an effective methodology for thermal activation of the Fe-SMA. Rapid heating techniques such as electrical resistance heating (ERH) prevent any significant heat transfer to the parent structure, minimise thermal strain development, and therefore lead to a higher recovery stress in the Fe-SMA element. Furthermore, it can be concluded that activation of the Fe-SMA elements under high stress levels (e.g., due to dead-load) will result in a reduced final recovery stress.

The values of the recovery stress in the present study are between 360MPa and 370MPa. These values are consistent with the results of previous studies (e.g., [9, 10, 28]) on activation of the Fe-SMA that have also employed a fully constrained thermal activation condition (i.e. total strain-controlled) with a heating rate of 2°C/min. Total strain-controlled thermal activa-

tion has been considered in the following for evaluation of the effect of cyclic loading on the mechanical response of the Fe-SMA.

4.4 Cyclic response of the Fe-SMA strips after activation

A set of 2% pre-strained Fe-SMA specimens were activated in total strain-control (with a temperature transient rate of 2°C/min) and were then subjected to cyclic loading. Figure 8 presents the observed initial stress-strain response of the activated Fe-SMA for different applied strains and strain rates. The early elastic deformation response demonstrates a modulus of 173GPa which is identical to that of the as-received material. The start of non-linear behaviour is dependent on the strain rate and advances with decreasing strain rate. Importantly, as shown in Figure 9, such non-linear deformation behaviour is responsible for a decrease in the subsequent recovery stress (i.e. after unloading, see $\sigma_{r,1}$ in Figure 9). The amount of recovery stress loss increases with increasing loading strain and decreasing strain rate (i.e. lower frequencies).

Repeating loading and unloading cycles further decreases the residual recovery stress in the Fe-SMA. Figure 10 presents the evolution of the observed maximum stress and recovery stress (i.e. minimum stress) for the first 10 cycles of deformation involving different strain ranges and frequencies. Figure 11 illustrates evolution of the residual recovery stress for the Fe-SMA for the different examined cyclic loading conditions up to two million loading cycles. It is observed that of the recovery stress reduced with cycle number at a decreasing rate and the reduction is more significant for cyclic loading conditions with larger strain ranges. Nevertheless, for the two strain ranges of 0.035% and 0.070%, which are relevant for service loading conditions [7, 9, 29], the recovery stress after two million cycles remained above 285MPa.

The observed loss of the recovery stress is attributed to cyclic-deformation-enhanced stress relaxation due to time-dependent inelastic deformation. As discussed in the next section, this

inelastic deformation is mostly due to austenite-to-martensite phase transformation rather than dislocation-induced plasticity. Such a decrease in the recovery stress is important and should be taken in to account in design assessments of SMA pre-stressed structures.

4.5 Second activation and subsequent cyclic loading

Relaxation of recovery stress during cyclic loading has been discussed in the previous section. The following examines employment of a second thermal activation process for retrieving at least a part of the relaxed recovery stress. For the tests with cyclic strain ranges of 0.070% and 0.105%, which showed considerable amounts of relaxation after two million cycles, the specimens were held under constant total-strain after the last cycle (at a strain level of ~1.3%). Similar to the first thermal activation process, the specimens were then heated to 160°C and cooled down to room temperature (at a rate of 2°C/min).

Figure 12 illustrates evolution of the stress in the Fe-SMA as a function of temperature during the second activation process. As can be seen, during the early stage of reheating and up to 70°C, the stress decreases substantially due to thermal expansion. With increasing temperature, the stress-temperature curve becomes less steep which is assumed to be a result of the shape memory effect and martensite-to-austenite transformation. During the cooling phase, the stress increases mainly due to thermal contraction. Figure 12 demonstrates that the second activation could effectively enhance the recovery stress in the Fe-SMA after cyclic deformation. A comparison of the obtained recovery stresses after the first and second activations indicates that the second activation retrieves a considerable portion of the recovery stress which had been relaxed due to cyclic loading. This phenomenon is more pronounced in particular for the specimen loaded for the strain range of 0.070% where the recovery stress at the end of the second activation is very close to that of the first activation. This indicates an almost full retrieval of the relaxed recovery stress and implies that the stress relaxation and accumulation of the inelastic strain during the cyclic loading are mainly due to the austenite-to-

12

martensite forward transformation, and therefore recoverable. Figure 13 shows the complete stress and temperature histories for specimen #8, including pre-straining, first activation, first cyclic loading, second activation, second cyclic loading and the final tensile loading.

The retrieval of relaxed recovery stress by a second activation has important implications for practical employment of the Fe-SMA as pre-stressing elements in civil engineering applications. Such reactivation, for example, can retrieve the pre-stressing force in a strengthened structure, when the SMA element has lost some of its pre-stressing force due to cyclic loading, relaxation or accidental overloading.

Figure 14 compares the behaviour of the Fe-SMA strips subjected to cyclic loading after the first and the second thermal activations. The observations indicate almost identical patterns in the stress relaxation behaviour of the Fe-SMA after first and second activations.

4.6 Final tensile loading

The last step for most of the conducted experiments in this study was applying an increasing tensile load to the specimens up to the failure. Figure 15 shows the tensile behaviour of the as-received specimen and those which were activated and subjected to cyclic loading. The results indicate that neither thermal activation nor cyclic loading (up to 2.2 million cycles) have induced any damage in the Fe-SMA to deteriorate the tensile response.

5. Concluding remarks

This study examined the mechanical behaviour of a novel Fe-SMA under different loading conditions. The following concluding remarks may help to better assess the integrity of structures employing this material, in particular those subjected to cyclic loading conditions.

- The as-received Fe-SMA strips showed outstanding tensile strength and elongation of >1'000MPa and >55%, respectively. These values were not affected by activation and subsequent cyclic loading (e.g. up to 2.2×10^6 cycles for $\Delta\varepsilon=0.105\%$).

- After 2% pre-straining, heating to 160°C and cooling to room temperature under total strain-control, the alloy recovers a stress of 360-370MPa. The finally recovered stress for activation under mechanical strain-control, where strains representative of the thermal expansion and contraction of the parent structure during heating and cooling are applied to the Fe-SMA during the activation process, is nearly half of that achieved under total strain-control. It can then be concluded that the tensile stress level on the Fe-SMA element during the activation process (thermal expansion of parent structure or due to dead-loads) should be minimized in order to obtain higher recovery stresses. Furthermore, this observation implies employment of fast heating methods such as the ERH technique for the thermal activation of Fe-SMA elements minimise the amount of heat transfer to parent structures and result in higher pre-stressing forces.

- The recovery stress partially relaxes when the activated Fe-SMA is subjected to cyclic loading conditions. The relaxation is more pronounced for larger strain ranges and lower strain rates. For the cyclic strain ranges relevant for practical applications of the Fe-SMA, the recovered stress remains above 280MPa after 2×10^6 cycles (e.g. for $\Delta\varepsilon = 0.07\%$ with frequency of 10Hz).

- A significant part of the loss in the recovery stress, which occurs during cyclic loading, is retrieved when the Fe-SMA is reheated to 160°C and cooled to room temperature (i.e., reactivation). Such observations indicate that relaxation of the recovery stress during cyclic deformation is mainly due to a forward phase transformation and is recoverable. This finding has important practical implications and provides a possible solution for restoring the pre-stressing force of structures, which have lost a substantial portion of their pre-stressing force due to relaxation, cyclic loading or overloading, simply by reheating the Fe-SMA elements to the activation temperature.

References

1. Cladera A., Weber B., Leinenbach C., Czaderski C., Shahverdi M., Motavalli M. Iron-based shape memory alloys for civil engineering structures: An overview. Construction and Building Materials, 2014. 63(0): p. 281-293.

2. Maruyama T., Kurita T., Kozaki S., Andou K., Farjami S., Kubo H. Innovation in producing crane rail fishplate using Fe–Mn–Si–Cr based shape memory alloy. Materials Science and Technology, 2008. 24(8): p. 908-912.

3. Czaderski C., Shahverdi M., Brönnimann R., Leinenbach C., Motavalli M. Feasibility of iron-based shape memory alloy strips for prestressed strengthening of concrete structures. Construction and Building Materials, 2014. 56(0): p. 94-105.

4. Sato A., Chishima E., Soma K., Mori T. Shape memory effect in $\gamma \rightleftarrows \epsilon$ transformation in Fe-30Mn-1Si alloy single crystals. Acta Metallurgica, 1982. 30(6): p. 1177-1183.

5. Czaderski C., Hahnebach B., Motavalli M. RC beam with variable stiffness and strength. Construction and Building Materials, 2006. 20(9): p. 824-833.

6. Mohd Jani J., Leary M., Subic A., Gibson M.A. A review of shape memory alloy research, applications and opportunities. Materials & Design (1980-2015), 2014. 56: p. 1078-1113.

7. Izadi M.R., Ghafoori E., Hosseini A., Motavalli M., Maalek S., Shahverdi M. Feasibility of iron-based shape memory alloy strips for prestressed strengthening of steel plates, in the fourth International Conference on Smart Monitoring, Assessment and Rehabilitation of Civil Structures (SMAR 2017). 2017: Zurich, Switzerland.

8. Dong Z., Klotz U.E., Leinenbach C., Bergamini A., Czaderski C., Motavalli M. A novel Fe-Mn-Si shape memory alloy with improved shape recovery properties by VC precipitation. Advanced Engineering Materials, 2009. 11(1-2): p. 40-44.

9. Lee W.J., Weber B., Feltrin G., Czaderski C., Motavalli M., Leinenbach C. Stress recovery behaviour of an Fe–Mn–Si–Cr–Ni–VC shape memory alloy used for prestressing. Smart Materials and Structures, IOP Science, 2013. 22: p. 1-9.

10. Lee W.J., Weber B., Feltrin G., Czaderski C., Motavalli M., Leinenbach C. Phase transformation behavior under uniaxial deformation of an Fe–Mn–Si–Cr–Ni–VC shape memory alloy. Materials Science and Engineering: A, 2013. 581: p. 1-7.

11. Leinenbach C., Kramer H., Bernhard C., Eifler D. Thermo-mechanical properties of an Fe-Mn-Si-Cr-Ni-VC shape memory alloy with low transformation temperature. Advanced Engineering Materials, 2012. 14(1-2): p. 62-67.

12. Lee W.J., Partovi-Nia R., Suter T., Leinenbach C. Electrochemical characterization and corrosion behavior of an Fe-Mn-Si shape memory alloy in simulated concrete pore solutions. Materials and Corrosion, 2016. 67(8): p. 839-846.

13. Leinenbach C., Lee W.J., Lis A., Arabi-Hashemi A., Cayron C., Weber B. Creep and stress relaxation of a FeMnSi-based shape memory alloy at low temperatures. Materials Science and Engineering A, 2016. 677: p. 106-115.

14. Michels J., Martinelli E., Czaderski C., Motavalli M. Prestressed CFRP strips with gradient anchorage for structural concrete retrofitting: Experiments and numerical modeling. Polymers, 2014. 6(1): p. 114-131.

15. Michels J., Sena-Cruz J., Czaderski C., Motavalli M. Structural strengthening with prestressed CFRP strips with gradient anchorage. Journal of Composites for Construction, 2013. 17(5): p. 651-661.

16. Ghafoori E., Motavalli M. Lateral-torsional buckling of steel I-beams retrofitted by bonded and un-bonded CFRP laminates with different pre-stress levels: experimental and numerical study. Construction and Building Materials, 2015. 76: p. 194–206.

17. Ghafoori E., Motavalli M., Botsis J., Herwig A., Galli M. Fatigue strengthening of damaged metallic beams using prestressed unbonded and bonded CFRP plates. International Journal of Fatigue, 2012. 44: p. 303-315.

18. Ghafoori E., Motavalli M., Nussbaumer A., Herwig A., Prinz G., Fontana M. Determination of minimum CFRP pre-stress levels for fatigue crack prevention in retrofitted metallic beams. Engineering Structures, 2015. 84: p. 29–41.

19. Ghafoori E., Motavalli M., Nussbaumer A., Herwig A., Prinz G.S., Fontana M. Design criterion for fatigue strengthening of riveted beams in a 120-year-old railway metallic bridge using pre-stressed CFRP plates. Composites Part B: Engineering, 2015. 68: p. 1-13.

20. Ghafoori E., Motavalli M. Innovative CFRP-Prestressing System for Strengthening Metallic Structures. Journal of Composites for Construction, 2015. 19(6): p. 04015006.

21. Kianmofrad F., Ghafoori E., Elyasi M.M., Motavalli M., Rahimian M. Strengthening of metallic beams with different types of pre-stressed un-bonded retrofit systems. Composite Structures, 2017. 159: p. 81-95.

22. Ghafoori E., Motavalli M. Flexural and interfacial behavior of metallic beams strengthened by prestressed bonded plates. Composite Structures, 2013. 101: p. 22-34.

23. Ghafoori E., Motavalli M., Zhao X.L., Nussbaumer A., Fontana M. Fatigue design criteria for strengthening metallic beams with bonded CFRP plates. Engineering Structures, 2015. 101: p. 542-557.

24. Ghafoori E., Schumacher A., Motavalli M. Fatigue behavior of notched steel beams reinforced with bonded CFRP plates: Determination of prestressing level for crack arrest. Engineering Structures, 2012. 45: p. 270-283.

25. Sawaguchi T., Nikulin I., Ogawa K., Sekido K., Takamori S., Maruyama T., Chiba Y., Kushibe A., Inoue Y., Tsuzaki K. Designing Fe–Mn–Si alloys with improved low-cycle fatigue lives. Scripta Materialia, 2015. 99: p. 49-52.

26. Sawaguchi T., Sahu P., Kikuchi T., Ogawa K., Kajiwara S., Kushibe A., Higashino M., Ogawa T. Vibration mitigation by the reversible fcc/hcp martensitic transformation during cyclic tension–compression loading of an Fe–Mn–Si-based shape memory alloy. Scripta Materialia, 2006. 54(11): p. 1885-1890.

27. Koster M., Lee W.J., Schwarzenberger M., Leinenbach C. Cyclic deformation and structural fatigue behavior of an FE–Mn–Si shape memory alloy. Materials Science and Engineering: A, 2015. 637(0): p. 29-39.

28. Lee W.J., Weber B., Leinenbach C. Recovery stress formation in a restrained Fe–Mn–Si-based shape memory alloy used for prestressing or mechanical joining. Construction and Building Materials, 2015. 95: p. 600-610.

29. Hosseini A., Ghafoori E., Motavalli M., Nussbaumer A., Zhao X.-L. Mode I fatigue crack arrest in tensile steel members using prestressed CFRP plates. Composite Structures, 2017. 178: p. 119-134.

30. Skibina L.V., Ilichev V.Y., Chernik M.M., V.P. P. Thermal expansion of the austenitic stainless steels and titanium alloys in the temperature range 5–300 K. Cryogenics, 1985. 25(1): p. 31-32.
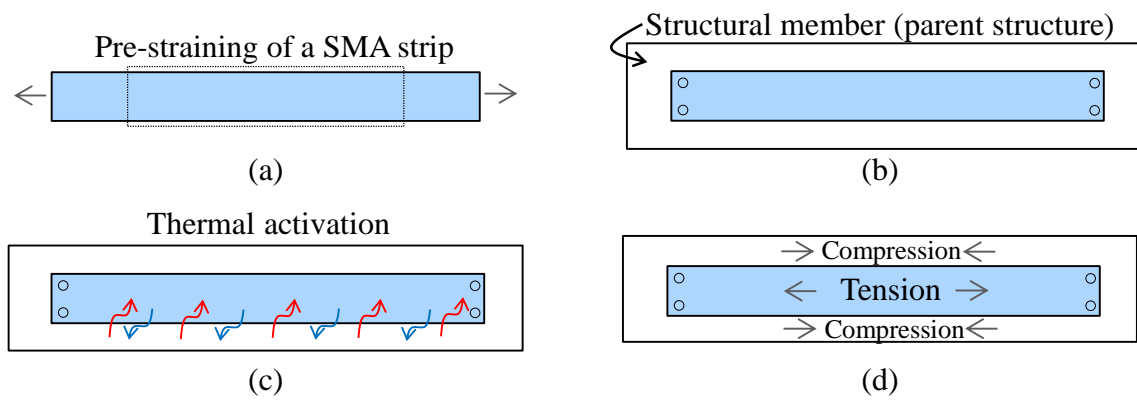
Figure and Tables

Fig. 1. Application of SMA elements to strengthen a structural member. a) pre-straining, b) fixing to a structural member c) thermal activation, d) stress state after activation.

Fig. 2. SEM-BSE image of the as-received Fe-SMA.

dog bone specimen

heating system

air cooling system

type-K thermocouple

side-entry extensometer
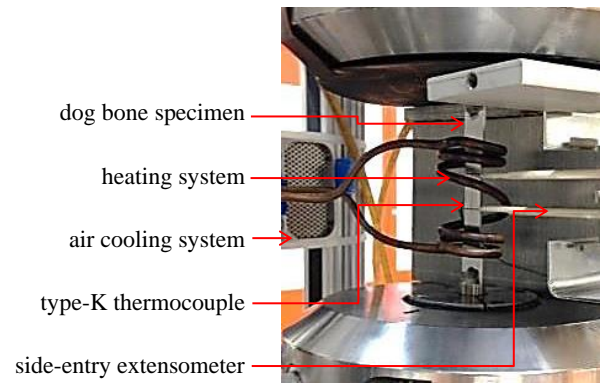
Fig. 3. Employed testing setup illustrating the dog-bone specimen, side-entry extensometer, thermocouple and heating/cooling systems.
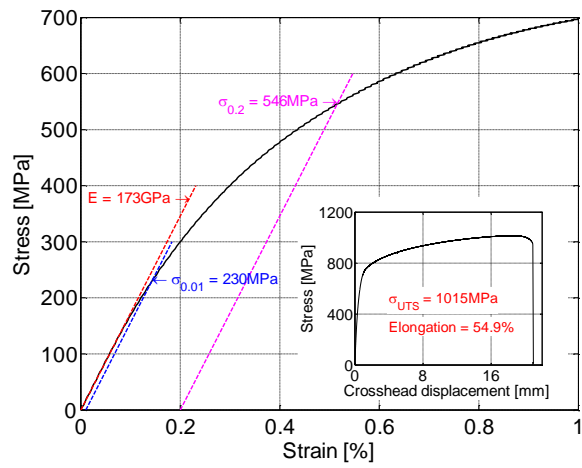
Fig. 4. Room temperature tensile behaviour of the as-received Fe-SMA.
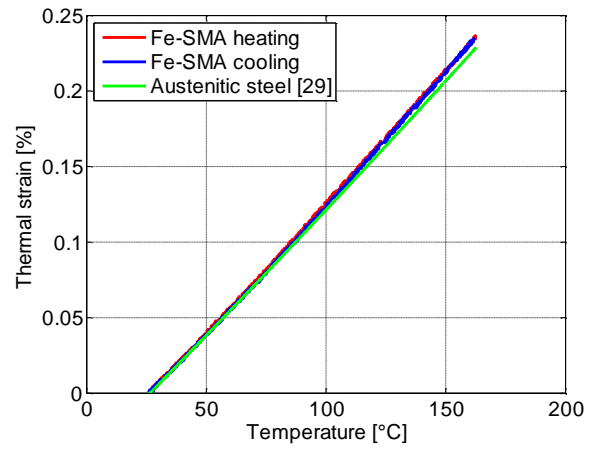
Fig. 5. Comparison between the thermal expansion behaviour of the as-received Fe-SMA in this study and that of a typical austenitic stainless steel [30].
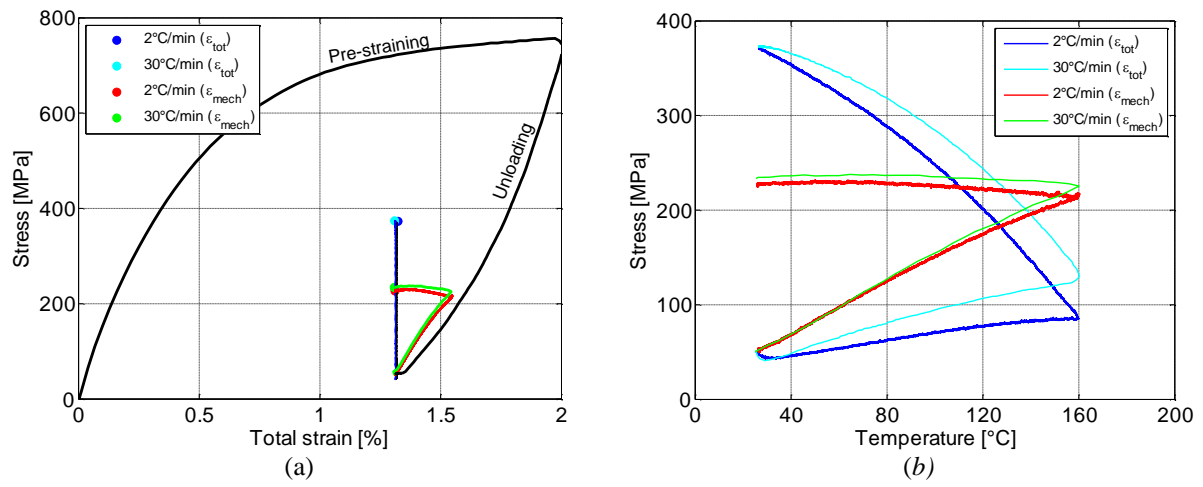
Fig. 6. (a) Stress as a function of the total strain during pre-straining and different thermal activation strategies. (b) Recovered stress in the Fe-SMA strip as a function of temperature for different thermal activation strategies.
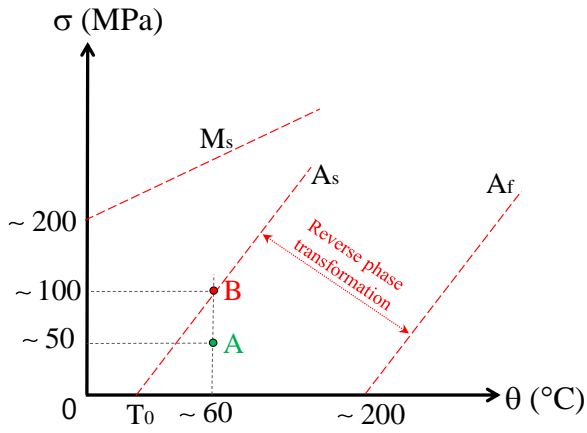
Fig. 7. Scheme of the stress-temperature phase diagram including A_s, A_f and M_s lines [10]. Coordinates A and B put into perspective the material phase state during total and mechanical strain controlled activation process during heating at T=60°C, respectively.
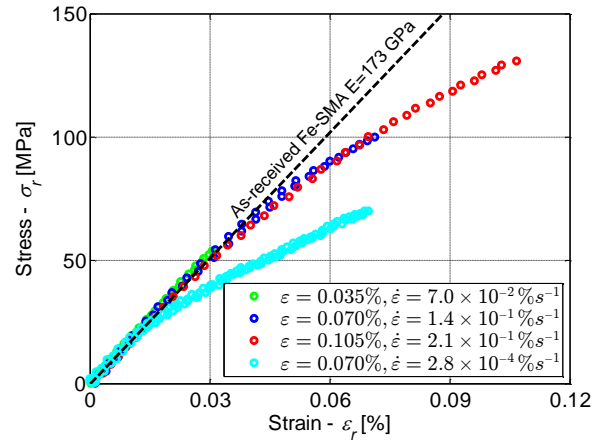
Fig. 8. The mechanical response of the activated Fe-SMA under tensile loading (σ_r =~360-370MPa and ε_r =~1.3% are stress and strain values at the end of thermal activation).
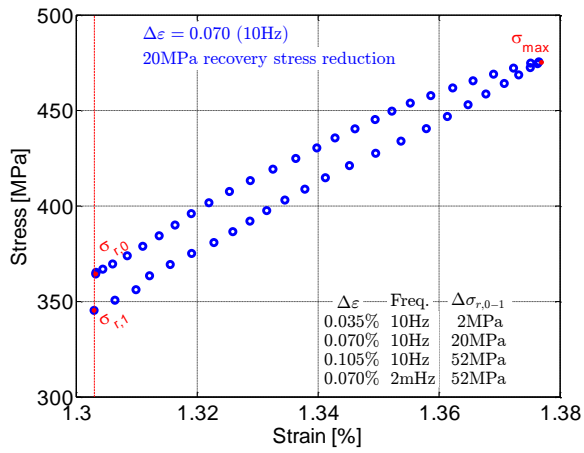
Fig. 9. Decrease of recovery stress due to the first loading and unloading cycle (0.070%, 10Hz) after activation of the Fe-SMA (inset: recovery stress reduction after first loading cycle for different conditions).
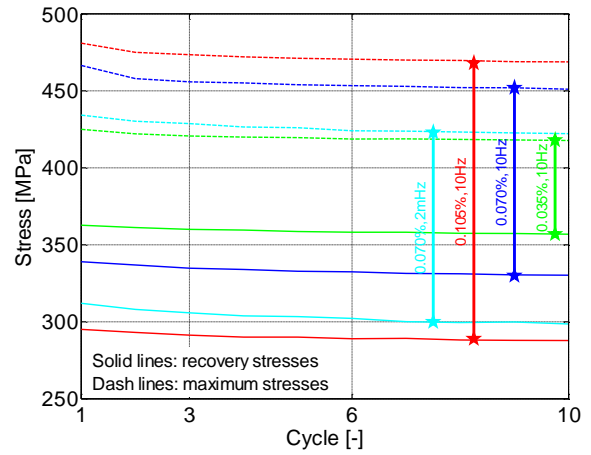
Fig. 10. Evolution of the recovery stress and the maximum stress in the activated Fe-SMA for the first ten load cycles for different strain ranges and frequencies
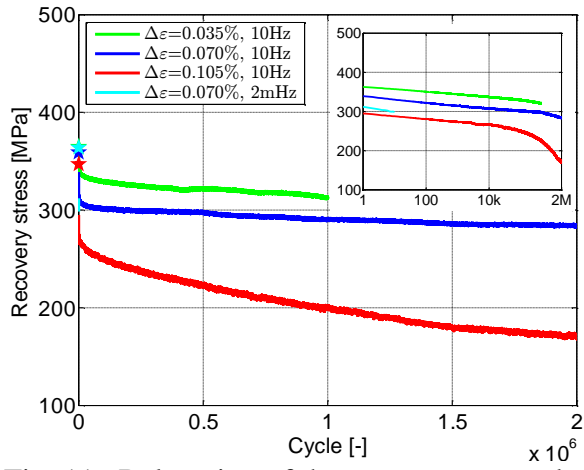
Fig. 11. Relaxation of the recovery stress due to cyclic loading of the activated Fe-SMA for different strain ranges and frequencies.
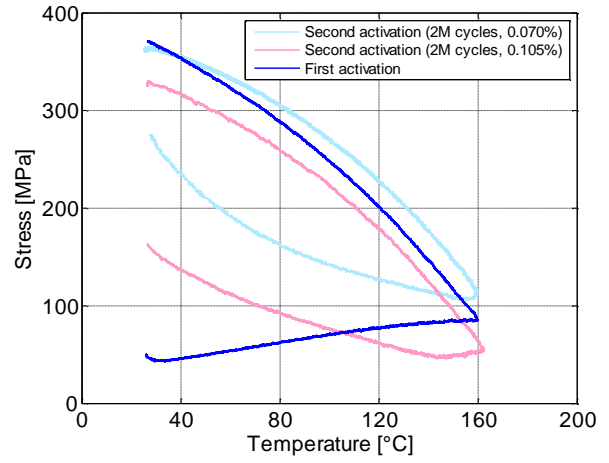

Fig. 12. Comparison of stress recovery behaviour during first and second thermal activations (after two million loading cycles).
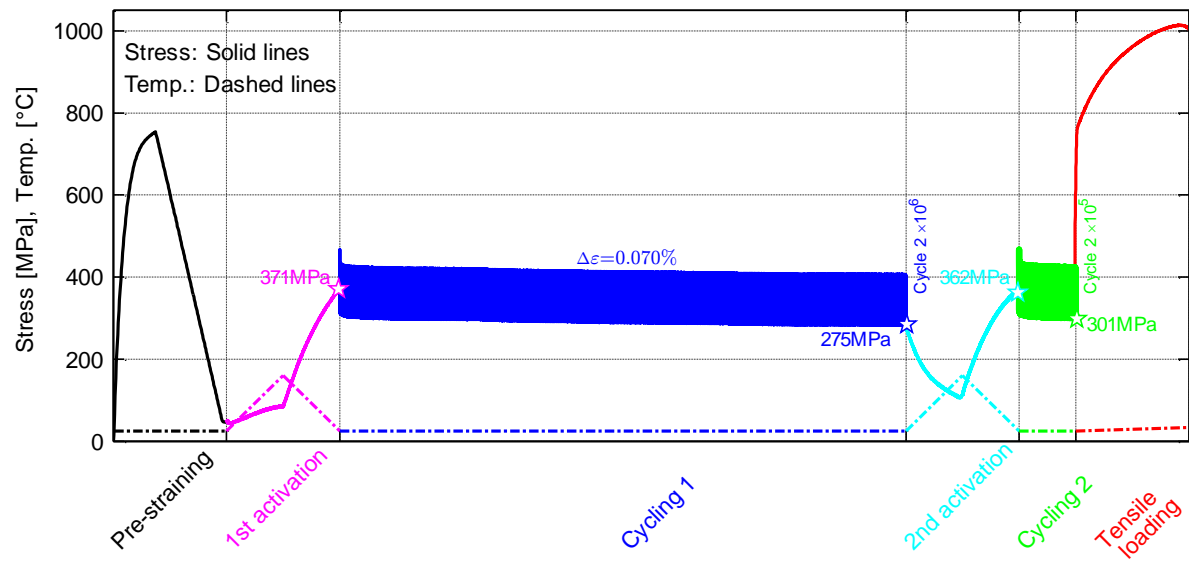
Fig. 13. Complete stress and temperature histories for specimen #8. The diagram includes different test steps of pre-straining, first activation, first cyclic loading, second activation, second cyclic loading and the final tensile loading.
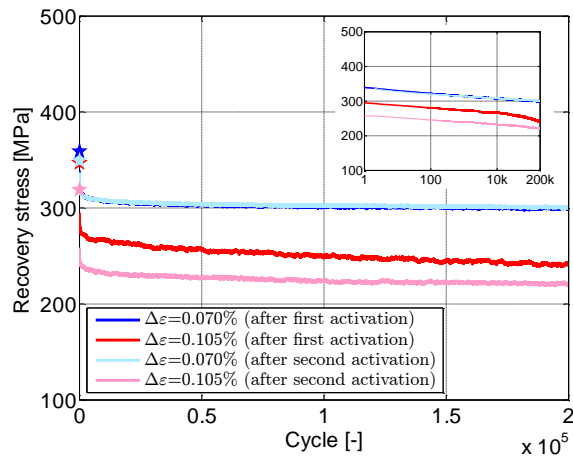
Fig. 14. Relaxation of recovery stress due to cyclic loading with different strain ranges for Fe-SMA after first and second thermal activations.
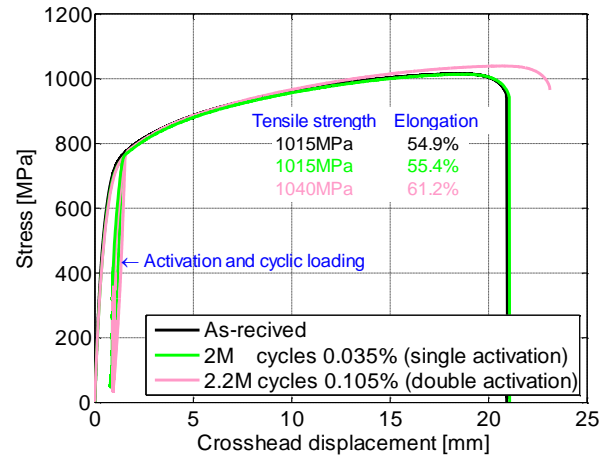

Fig. 15. Tensile behaviour of the as-received Fe-SMA in comparison with those after activation and cyclic loading.

Table 1. Summary of the conducted experiments.

Specimen	Testing detail
#1	Uniaxial room temperature tensile testing
#2	Determination of thermal expansion response
#3	Pre-straining and mechanical strain-controlled thermal activation (30°C/min)
#4	Pre-straining and mechanical strain-controlled thermal activation (2°C/min)
#5	Pre-straining and total strain-controlled thermal activation (30°C/min)
#6	Pre-straining and total strain-controlled thermal activation (2°C/min), followed by cyclic deformation (10 cycles, 2mHz, $\Delta\varepsilon$=0.070%)
#7	Pre-straining and total strain-controlled thermal activation (2°C/min), cyclic deformation (2×10^6 cycles, 10Hz, $\Delta\varepsilon$=0.035%) and final tensile testing
#8	Pre-straining and total strain-controlled thermal activation (2°C/min), cyclic deformation (2×10^6 cycles, 10Hz, $\Delta\varepsilon$=0.070%), reactivation (2°C/min), cyclic deformation (2×10^5 cycles, 10Hz, $\Delta\varepsilon$=0.070%) and final tensile loading
#9	Pre-straining and total strain-controlled thermal activation (2°C/min), cyclic deformation (2×10^6 cycles, 10Hz, $\Delta\varepsilon$=0.105%), reactivation (2°C/min), cyclic deformation (2×10^5 cycles, 10Hz, $\Delta\varepsilon$=0.105%) and final tensile loading